

Spin-dependent observables and the D_2 parameter in breakup of deuteron and ^3He

A. P. Kobushkin^{1,a} and E.A. Strokovsky^{2,b}

¹ Bogolyubov Institute for Theoretical Physics, Metrologicheskaya Street 14B, 03680 Kiev, Ukraine; and National Technical University of Ukraine “KPI”, Prospekt Peremogy 37, 03056 Kiev, Ukraine.

² Joint Institute for Nuclear Research, Laboratory of High Energy Physics, 141980, Dubna, Russia.

Abstract. We analyze the momentum distributions of constituents in ^3He , as well as the spin-dependent observables for $(^3\text{He}, d)$, $(^3\text{He}, p)$, and (d, p) breakup reactions. Special attention is paid to the region of small relative momenta of the helium-3 and the deuteron constituents, where a single parameter, D_2 , has determining role for the spin-dependent observables. We extract also this parameter for the deuteron, basing on existing data for the tensor analyzing power of this reaction.

1 Introduction

Momentum distributions of one and two nucleon fragments in the lightest nuclei such as ^3He and deuteron give important information about nuclear system structure. They cast light on such interesting problems as the nucleon-nucleon interaction at short distances, the role of three-body interaction (the $3N$ -forces in the ^3He case), and non-nucleonic degrees of freedom in nuclei. Data on spin-dependent observables contain an important complementary information to this.

Precise data are currently available on the momentum distributions of the proton and the deuteron in ^3He obtained with electromagnetic [1,2,3,4] and hadronic probes [5,6,7]. Data on the energy dependence of the differential cross sections of backward elastic $^3\text{He}(p, ^3\text{He})p$ scattering, which are related to the same momentum distributions, also exist [8,9]. Furthermore, the spin-correlation parameter C_{yy} for this reaction was recently measured for first time [9]. Finally, the tensor polarization of the deuteron in the $^{12}\text{C}(^3\text{He}, d)$ reaction was also measured [10,11]. Both this and the C_{yy} data [9] are sensitive to the spin structure of ^3He .

A convenient parametrization of the fully antisymmetric three-nucleon wave function based on the Paris [12] and CD-Bonn [13] potentials has been presented [14]. We used it in Ref. [15] in order to calculate the momentum distributions in ^3He , as well as the spin-dependent observables, within the framework of the spectator model for the ^3He breakup reactions. We paid in [15] special attention to the study of the two-body $^3\text{He} \rightarrow d + p$ channel and compared our results with other theoretical works and existing experimental data.

^a e-mail: kobushkin@bitp.kiev.ua

^b e-mail: strok@sunse.jinr.ru

In our analysis [15] of spin-dependent observables for $(^3\text{He}, d)$ and $(^3\text{He}, p)$ reactions, we carefully consider their behavior in the region of small (below $\approx 150 \text{ MeV}/c$) internal momenta of the ${}^3\text{He}$ fragments, where a single quantity, known in the literature as the D_2 parameter, completely determines both the sign and the momentum dependence of the observables.

Similar parameter is known for the bound $2N$ system (the deuteron) as well. It determines the behavior of spin-dependent observables for the (d, p) breakup in the same sense as for the ${}^3\text{He}$ case, but for the (d, p) breakup rather good database exists what makes possible an independent extraction of this parameter. We performed here the corresponding analysis; the obtained result agrees well with existing theoretical values as well as with experimental estimations, extracted from low energy reactions.

2 The parametrization of the three-nucleon wave function

We here give a brief review of the parametrization of the ${}^3\text{He}$ wave function [14]. Working in the framework of the so-called channel spin coupling scheme (Ref. [16]), the authors of Ref. [14] restricted themselves to five partial waves

$$|[(\ell s)j\frac{1}{2})KL]\frac{1}{2}\rangle, \quad (1)$$

where ℓ , j and s are the orbital, total, and spin angular momenta for the pair (the 2nd and 3rd nucleons), L and K are relative orbital angular momentum for the spectator (the 1st nucleon) and the channel spin, respectively. Coulomb effects are not included. The appropriate quantum numbers of the partial waves are collected in Table 1.

We use the standard definition of the Jacobi coordinates \mathbf{r} (the relative coordinate between nucleons in the pair) and $\boldsymbol{\rho}$ (the relative coordinate between the nucleon-spectator and the pair) with the corresponding momenta being \mathbf{p} and \mathbf{q} .

Explicitly, the wave function of ${}^3\text{He}$ in momentum space, normalized to unity, reads (see also Ref. [15]):

$$\begin{aligned} \Psi_\sigma(\mathbf{p}, \mathbf{q}) = & \sum_\xi \left\{ \frac{1}{4\pi} \delta_{\xi\sigma} \sum_{\tau_3, t_3} \langle 1\frac{1}{2}\tau_3 t_3 | \frac{1}{2}\frac{1}{2} \rangle \psi_1(p, q) |00; 1\tau_3\rangle \chi_{\xi t_3} \right. \\ & + \sum_{s_3} \left[\frac{1}{4\pi} \langle 1\frac{1}{2}s_3 \xi | \frac{1}{2}\sigma \rangle \psi_2(p, q) - \sqrt{\frac{1}{4\pi}} \sum_{L_3 K_3} \langle 1\frac{1}{2}s_3 \xi | \frac{3}{2}K_3 \rangle \langle \frac{3}{2}2K_3 L_3 | \frac{1}{2}\sigma \rangle \right. \\ & \times Y_{2L_3}(\hat{\mathbf{q}}) \psi_3(p, q) - \sqrt{\frac{1}{4\pi}} \sum_{\ell_3 M} \langle 12s_3 \ell_3 | 1M \rangle \langle 1\frac{1}{2}M \xi | \frac{1}{2}\sigma \rangle Y_{2\ell_3}(\hat{\mathbf{p}}) \psi_4(p, q) \quad (2) \\ & + \sum_{\ell_3 M L_3 K_3} \langle 12s_3 \ell_3 | 1M \rangle \langle 1\frac{1}{2}M \xi | \frac{3}{2}K_3 \rangle \langle \frac{3}{2}2K_3 L_3 | \frac{1}{2}\sigma \rangle Y_{2L_3}(\hat{\mathbf{q}}) Y_{2\ell_3}(\hat{\mathbf{p}}) \\ & \left. \times \psi_5(p, q) \right] |1s_3; 00\rangle \chi_{\xi \frac{1}{2}} \left. \right\}, \end{aligned}$$

where σ and ξ are the spin projections of ${}^3\text{He}$ and the nucleon-spectator, t_3 is the isospin projection of the nucleon-spectator, M is the projection of the total angular momentum of the pair, $\chi_{\xi t_3}$ and $|ss_3; \tau\tau_3\rangle$ are the spin-isospin wave function of the spectator nucleon and the pair, respectively.

The values of the partial channel probabilities, defined as $P_\nu = \frac{1}{3} \int d^3q \rho_\nu(q) = \int dp dq p^2 q^2 |\psi_\nu(p, q)|^2$, are given in the last two columns of Table 1.

Table 1. Quantum numbers of the ${}^3\text{He}$ partial waves. Here s , τ , ℓ and j are spin, isospin, orbital and total angular momenta of the pair; L and K are relative angular momenta for the spectator and the channel spin, respectively.

Channel #	Label	ℓ	s	j^π	K	L	τ	P_ν	
								Paris	CD-Bonn
1	1s_0S	0	0	0^+	$1/2$	0	1	0.5000	0.5000
2	3s_1S	0	1	1^+	$1/2$	0	0	0.4600	0.4658
3	3s_1D	0	1	1^+	$3/2$	2	0	0.0282	0.0231
4	3d_1S	2	1	1^+	$1/2$	0	0	0.0103	0.0102
5	3d_1D	2	1	1^+	$3/2$	2	0	0.0015	0.0009

It is important to note that the distributions for the 1s_0S and 3s_1S channels are very similar in both their magnitude and their momentum dependence.

We use the following convention for angular momentum summation in Eq. (2):

$$j + \frac{1}{2} \rightarrow K, \quad K + L \rightarrow \frac{1}{2}. \quad (3)$$

Other conventions are often used in the literature, for example:

$$j + \frac{1}{2} \rightarrow K, \quad L + K \rightarrow \frac{1}{2}, \quad (4)$$

$$\frac{1}{2} + j \rightarrow K, \quad L + K \rightarrow \frac{1}{2}. \quad (5)$$

The convention of Eq. (4) was used, in particular, in Ref. [17], whereas that of Eq. (5) was exploited in Ref. [18].

Due to the properties of the Clebsch–Gordan coefficients under permutations, some of the wave function components have opposite signs in different conventions. For example, using Eq. (4) rather than Eq. (3) would result in $\psi_3(p, q) \rightarrow -\psi_3(p, q)$ and $\psi_5(p, q) \rightarrow -\psi_5(p, q)$. Similarly, the use of Eq. (5) instead of Eq. (3) would give $\psi_2(p, q) \rightarrow -\psi_2(p, q)$, $\psi_3(p, q) \rightarrow -\psi_3(p, q)$, $\psi_4(p, q) \rightarrow -\psi_4(p, q)$, and $\psi_5(p, q) \rightarrow -\psi_5(p, q)$, while $\psi_1(p, q)$ would not change sign.

3 Momentum distributions

3.1 One-nucleon distributions

The momentum distribution of a nucleon N with spin and isospin projections ξ and t_3 in ${}^3\text{He}$ with spin projection σ is

$$N_{\sigma(\xi t_3)}(\mathbf{q}) = 3 \sum_{ss_3\tau\tau_3} \int d^3p \left| \langle ss_3\tau\tau_3 | \Psi_\sigma(\mathbf{p}, \mathbf{q}) \rangle \right|^2. \quad (6)$$

In the neutron case, Eq. (6) reduces to $n_{\sigma\xi}(q) = \frac{2}{3}\delta_{\sigma\xi}\rho_1(q) \equiv \delta_{\sigma\xi}n(q)$; the number of neutrons in ${}^3\text{He}$ is $\mathcal{N}_n = \int d^3q n(q) = 1$, so the ψ_1 component must be normalized as $\int dp dq p^2 q^2 [\psi_1(p, q)]^2 = 1/2$. Here and below we use $p_{\sigma\xi}$ and $n_{\sigma\xi}$ instead of $N_{\sigma(\xi, \frac{1}{2})}$ and $N_{\sigma(\xi, -\frac{1}{2})}$, respectively.

The momentum distribution of the proton, given by the sum of $p_{\frac{1}{2}\frac{1}{2}}(q, \theta)$ and $p_{\frac{1}{2}-\frac{1}{2}}(q, \theta)$ (where $p_{\frac{1}{2}\frac{1}{2}}(q, \theta)$ and $p_{\frac{1}{2}-\frac{1}{2}}(q, \theta)$ are the momentum distributions of protons with spin projection $\frac{1}{2}$ and $-\frac{1}{2}$ in the ${}^3\text{He}$ having spin projection $+\frac{1}{2}$) is:

$$p(q) = \frac{1}{3}\rho_1(q) + \rho_2(q) + \rho_3(q) + \rho_4(q) + \rho_5(q). \quad (7)$$

The number of protons in ${}^3\text{He}$ is $\mathcal{N}_p = \int d^3q p(q) = 2$ (see Ref. [15]).

3.2 Two-nucleon momentum distributions

We define the two-body amplitudes $A_{dp}(M, \xi, \sigma, \mathbf{q})$ as

$$\begin{aligned} A_{dp}(M, \xi, \sigma, \mathbf{q}) &= (2\pi)^{\frac{3}{2}} \sqrt{3} \int d^3 p \psi_d^\dagger(M, \mathbf{p}) \chi_{\xi \frac{1}{2}}^\dagger \Psi_\sigma(\mathbf{p}, \mathbf{q}) \quad (8) \\ &= (2\pi)^{\frac{3}{2}} \left\{ \sqrt{\frac{1}{4\pi}} \langle 1\frac{1}{2}M\xi | \frac{1}{2}\sigma \rangle u(q) - \sum_{K_3 L_3} \langle 1\frac{1}{2}M\xi | \frac{3}{2}K_3 \rangle \langle 2\frac{3}{2}L_3 K_3 | \frac{1}{2}\sigma \rangle Y_{2L_3}(\hat{q}) w(q) \right\}, \end{aligned}$$

where $\sqrt{3}$ is the spectroscopic factor, $\psi_d(M, \mathbf{p})$ is the deuteron wave function in momentum space, M and ξ are spin projections of the deuteron and the proton and

$$\begin{aligned} u(q) &= \sqrt{3} \int_0^\infty dp p^2 [u_d(p) \psi_2(p, q) + w_d(p) \psi_4(p, q)], \\ w(q) &= -\sqrt{3} \int_0^\infty dp p^2 [u_d(p) \psi_3(p, q) + w_d(p) \psi_5(p, q)]; \end{aligned} \quad (9)$$

here $u_d(p)$ and $w_d(p)$ are the deuteron S and D wave functions, respectively¹. The momentum distribution of the deuteron in ${}^3\text{He}$ is $d(q) = u^2(q) + w^2(q)$.

The effective numbers of the deuterons in ${}^3\text{He}$, $\mathcal{N}_d = \int d^3 q q^2 d(q)$, are 1.39 and 1.36 for the Paris and CD-Bonn potentials. These can be compared with $\mathcal{N}_d = 1.38$ obtained in variational calculations [19] with both the Argonne and Urbana potentials. The probabilities of the D -wave in the $d + p$ configuration are 1.53 % and 1.43 % for the Paris and CD-Bonn potentials, respectively.

4 Spin-dependent observables

4.1 Tensor analyzing powers and the D_2 parameter

In a plane wave Born approximation the tensor analyzing powers T_{20} , T_{21} and T_{22} of the (d, t) and $(d, {}^3\text{He})$ reactions at low energies are determined by a single parameter, D_2 , used, for example, in Refs. [17,21,22,23]: $D_2 = \lim_{q \rightarrow 0} w(q)/[q^2 u(q)]$, i.e., $w(q)/u(q) \approx q^2 D_2$ at small q . The D_2 parameter is closely related to the asymptotic D to S ratio for the $p + d$ partition of the ${}^3\text{He}$ wave function, as is noted in Ref. [23].

The spin-dependent observables considered here depend upon the bilinear forms of S and D waves of the ${}^3\text{He}$ wave function and the behavior of their ratio at small q is completely governed by the D_2 parameter. In Table 2 we compare this parameter, calculated for the bound $3N$ system (using the wave functions based on different potentials) with the value derived from experiment.

Table 2. $D_2(3N)$ parameter (in fm²).

Paris	CD-Bonn	AV18 [19]	Urbana [19]	experiment [23]
-0.2387	-0.2487	-0.27	-0.23	-0.259 ± 0.014

4.2 Tensor polarization of the deuteron

We start by considering the tensor polarization ρ_{20} of the deuteron in $({}^3\text{He}, d)$ breakup. The quantization axis is chosen along the deuteron momentum, i.e., $\mathbf{q} = (0, 0, -q)$. We obtain (see also Ref. [15] for details) within the spectator model, that

$$\rho_{20} = -\frac{1}{\sqrt{2}} \frac{2\sqrt{2}u(q)w(q) + w^2(q)}{u^2(q) + w^2(q)}; \text{ at small } q: \rho_{20} \approx -2 \frac{w(q)}{u(q)} = -2q^2 D_2. \quad (10)$$

¹ For the convention given by Eq. (4) one must replace $w(q)$ by $-w(q)$. This notation was used, e.g., in Ref. [20].

Results of calculations are given in Fig. 1 (the left panel).

Note that even in the case of the breakup of an unpolarized ${}^3\text{He}$, the deuteron spectator emitted at 0° has a tensor polarization.

4.3 Polarization transfer from ${}^3\text{He}$ to d

We consider here the case when the quantization axes for the ${}^3\text{He}$ and the deuteron are parallel and both are perpendicular to the deuteron momentum. In this case the coefficient of the vector-to-vector polarization transfer from polarized ${}^3\text{He}$ to deuteron is (see Ref. [15])

$$\kappa_d = \frac{2}{3} \cdot \frac{u^2(q) - w^2(q) - u(q)w(q)/\sqrt{2}}{u^2(q) + w^2(q)} . \quad (11)$$

We point out that the expression given in Eq. (11) differs from Eq. (5) of Ref. [25] by a factor 2 (erroneously lost in Ref. [25]).

Results of calculations for κ_d are shown in Fig. 1 (the right panel).

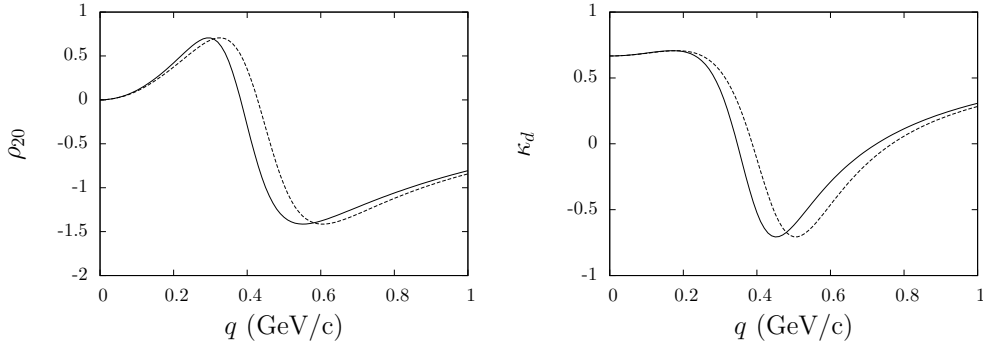


Fig. 1. Tensor polarization of the deuteron in ${}^3\text{He}$ (left) and polarization transfer κ_d from ${}^3\text{He}$ to d (right). Solid and dashed lines are for the Paris and CD-Bonn potentials.

The observables κ_d and ρ_{20} are related by: $\left(\frac{3}{2}\kappa_d\right)^2 + \left(\rho_{20} + \frac{1}{2\sqrt{2}}\right)^2 = 9/8$. Furthermore, at small q

$$\kappa_d \approx \frac{2}{3} \left(1 - \frac{q^2 D_2}{\sqrt{2}}\right) \approx \frac{2}{3} \left(1 + \frac{\rho_{20}}{2\sqrt{2}}\right) , \text{ i.e. } \kappa_d \rightarrow 2/3 \text{ when } q \rightarrow 0 . \quad (12)$$

4.4 Polarization transfer from ${}^3\text{He}$ to p

The polarization transfer from ${}^3\text{He}$ to p is defined by:

$$\kappa_p = \frac{p_{\frac{1}{2}\frac{1}{2}} - p_{\frac{1}{2}-\frac{1}{2}}}{p_{\frac{1}{2}\frac{1}{2}} + p_{\frac{1}{2}-\frac{1}{2}}} , \quad (13)$$

($p_{\sigma\xi}$ are defined in the subsection 3.1; details are in [15]). At $\theta = 90^\circ$ this reduces to

$$\kappa_p = \frac{\rho_1 - \rho_2 - \rho_4 - 2(\rho_3 + \rho_5) + 2\sqrt{2}(\rho_{13} + \rho_{45})}{\rho_1 + 3(\rho_2 + \rho_3 + \rho_4 + \rho_5)} , \quad (14)$$

where $\rho_{\mu\nu}(q) = [3/(4\pi)] \int_0^\infty dp p^2 \psi_\mu(p, q) \psi_\nu(p, q)$.

It is interesting to compare (14) with the polarization transfer for the $d + p$ projection of the ${}^3\text{He}$ wave function (see Fig. 2):

$$\tilde{\kappa}_p = -\frac{1}{3} \cdot \frac{u^2(q) + 2\sqrt{2}u(q)w(q) + 2w^2(q)}{u^2(q) + w^2(q)}. \quad (15)$$

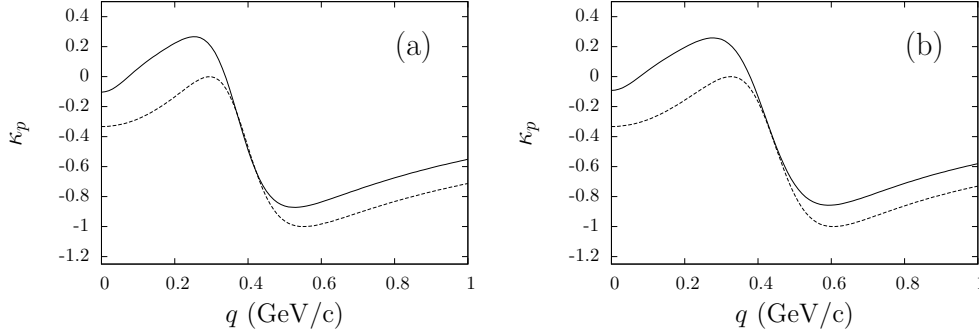


Fig. 2. The coefficient of polarization transfer from ${}^3\text{He}$ to the proton. The ${}^3\text{He}$ wave function used is based on the Paris potential (a) and CD-Bonn potential (b). Solid line: full wave function; short-dashed line: only the $d + p$ projection (i.e., the $\tilde{\kappa}_p$).

It is easy to see that the observables $\tilde{\kappa}_p$ and ρ_{20} must be related because they are determined by the ratio of the two functions $u(q)$ and $w(q)$. One then finds [15]:

$$\tilde{\kappa}_p = -\frac{1}{3} \left(1 - \sqrt{2}\rho_{20} \right); \text{ at small } q: \tilde{\kappa}_p \approx -\frac{1}{3} \left(1 - 2\sqrt{2}q^2 D_2 \right) \rightarrow -\frac{1}{3} \text{ at } q \rightarrow 0. \quad (16)$$

A linear combination of the two polarization transfer coefficients at small q is:

$$1 - (\tilde{\kappa}_p + 2\kappa_d) \approx 3q^4(D_2)^2 \approx \frac{3}{4}(\rho_{20})^2. \quad (17)$$

By the way, the similar coefficient of polarization transfer from ${}^3\text{He}$ to the neutron, i.e. κ_n , is equal to 1 in the spectator model.

5 Comparison with experiment

5.1 Empirical momentum distributions

In order to compare the calculated momentum distributions as well as the spin-dependent observables with experiment, it is necessary to establish a correspondence between the argument \mathbf{q} of the ${}^3\text{He}$ wave function and the measured spectator momentum. This must be done in a way that allows one to take into account relativistic effects in ${}^3\text{He}$. This problem was discussed in our paper [15] and here we follow to prescriptions formulated there on the basis of so-called “light front dynamics”.

Using the corresponding relations, one can extract the relevant momentum distributions from the measured cross sections; we call such extracted momentum distributions as “empirical momentum distributions” (EMDs) of the spectators in ${}^3\text{He}$.

In Fig. 3 we show EMDs for protons and deuterons in ${}^3\text{He}$ extracted from ${}^{12}\text{C}({}^3\text{He},p)$ and ${}^{12}\text{C}({}^3\text{He},d)$ breakup data, obtained for fragments, emitted at zero angle and at $p_{\text{He}} = 10.8 \text{ GeV}/c$ [5]. They are compared with the results of our calculations and with available results of other experiments. Good agreement between the

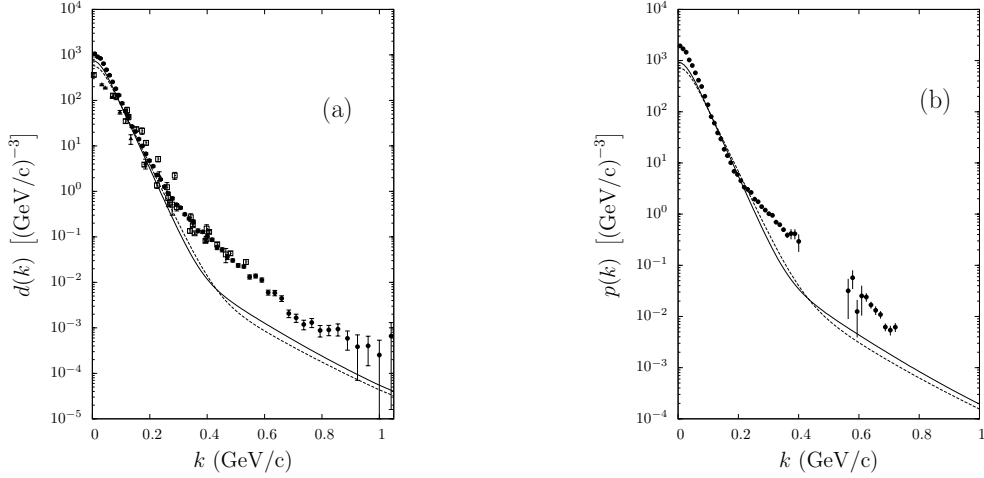


Fig. 3. The empirical momentum distributions (EMDs) of deuterons (a) and protons (b) in ${}^3\text{He}$. The solid and dashed lines are calculated with the Paris and CD-Bonn potentials. Abscissa: the light cone variable k , representing the argument q of the ${}^3\text{He}$ wave function. Full circles: the EMD extracted from Ref. [5]. Squares and triangles represent data extracted from Refs. [6] and [7]. The EMD for protons is normalized to the calculated one for $k < 100 \text{ MeV}/c$.

data and the calculations is obvious at small $k \lesssim 0.25 \text{ GeV}/c$, which indicates that in this region the spectator model can be used for data interpretation. Note that the difference between the light cone variable k and the spectator momentum, taken in the ${}^3\text{He}$ rest frame, is small in this region.

There is an enhancement of the extracted EMDs over theoretical curves at very small $k \lesssim 50 \text{ MeV}/c$. A natural explanation of this enhancement appears to be a manifestation of Coulomb effects, which we neglect here, as well as any possible final state interaction between the outgoing proton and deuteron, following to [15].

It was argued in Refs. [5] and [15] that the k -variable is an adequate measure for the internal relative momentum of the ${}^3\text{He}$ constituents. Data on the (d, p) breakup [26], including those for spin-dependent observables [27,28] and their analysis, have resulted in similar conclusions: at small $k \lesssim 0.25 \text{ GeV}/c$ the spectator model can be used for the data analysis. Thus we expect that the reliability of the spectator model for the ${}^3\text{He}$ breakup at $k \lesssim 250 \text{ MeV}/c$ should be the same as in the (d, p) case.

The data points for momenta above $k \approx 0.25 \text{ GeV}/c$, where the distances between the ${}^3\text{He}$ constituents become comparable to the nucleon radius or even less, systematically exceed the calculated momentum distributions. This is once again very similar to the excess of data over calculations in the (d, p) breakup [26]. It is possible that the observed enhancements in $({}^3\text{He}, d)$ and $({}^3\text{He}, p)$ reactions have the same nature.

5.2 Tensor polarization of the deuteron

Data on the tensor polarization ρ_{20} of the deuteron in the reaction ${}^{12}\text{C}({}^3\text{He}, d)$ at several GeV have been published in [10,11]. It should, however, be noted that the preliminary data [11] of this experiment have the opposite sign to those tabulated in the final data set [10].

On the other hand, the experimental value of the D_2 parameter for ${}^3\text{He}$ projected onto the $d + p$ channel has the opposite sign with respect to the experimental data on the similar D_2^d parameter for the deuteron in the $n + p$ channel. Therefore the sign of the ρ_{20} under discussion must be opposite to that of the tensor analyzing power in

the (d, p) breakup. Taking this into account, together with the contradiction in signs of ρ_{20} between Refs. [11] and [10], it is tempting to conclude that the data tabulated in Ref. [10] have the wrong sign. We therefore use the data from Ref. [10] but with a reversed sign and compare them in Fig. 4 with ρ_{20} calculated according Eq. (10).

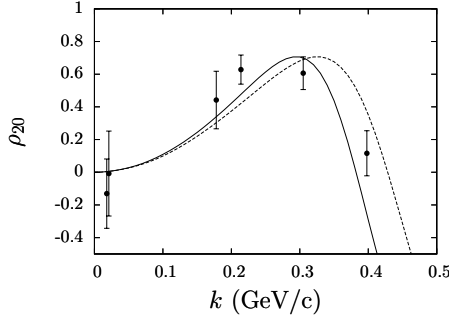


Fig. 4. Deuteron tensor polarization ρ_{20} calculated with the ${}^3\text{He}$ wave functions for the Paris (solid) and CD-Bonn (dashed) potentials compared with experimental data. The signs of the data points [10] are reversed to bring them into accordance with the preliminary results [11] of the same experiment, as well as with the sign of experimental data on the D_2 parameter for ${}^3\text{He}$.

Our results for other spin-dependent observables in the ${}^3\text{He}$ breakup cannot currently be compared with experiment because at the present time there are no polarized ${}^3\text{He}$ beams with energies of several GeV/nucleon.

5.3 Tensor analyzing power in the deuteron breakup

For the (d, p) breakup reaction with proton emitted at 0° , considered within the same scheme as in Sect. 4, it is possible to connect corresponding spin-dependent observables with parameter D_2^d defined by the same equation as for the ${}^3\text{He}$ case, where $u_d(q)$ and $w_d(q)$ functions are the S and D waves of the bound $p + n$ system. It is straightforward to see that for the analyzing power T_{20} and the polarization transfer coefficient κ_0 at small k one has

$$T_{20} \approx -2k^2 D_2^d \quad \text{and} \quad \kappa_0 \approx \left(1 + \frac{1}{\sqrt{2}}k^2 D_2^d\right) \approx 1 - \frac{1}{2\sqrt{2}}T_{20}. \quad (18)$$

The T_{20} data published in [27,28] are accurate enough in order to use Eq. (18) for estimation of the D_2^d parameter (Fig. 5).

Fit of the T_{20} data for $p(d, p)X$ reaction in the region of $k \leq 0.15 \text{ GeV}/c$ gives $2D_2^d = +(23.70 \pm 0.33) (\text{GeV}/c)^{-2}$ with $\chi^2/\text{DoF} = 19.7/12$ (the Dubna data are not included in the fit as well as two Saclay data points at $k \approx 74$ and $106 \text{ MeV}/c$).

The obtained value of $2D_2^d = +(23.7 \pm 0.33) (\text{GeV}/c)^{-2}$ should be compared with values published in [17]: $2D_2^d = +(22.19 \pm 0.82) (\text{GeV}/c)^{-2}$ and in [30]: $2D_2^d = +(24.80 \pm 0.67) (\text{GeV}/c)^{-2}$. Theoretical estimations of this parameter (in $(\text{GeV}/c)^{-2}$ units) can be found, for example, in papers [24],[29] for different NN potentials (in the paper by E. Epelbaum [24] the estimations are based on the chiral EFT calculations in $N^3\text{LO}$); all of them are in the interval from $+24.07$ to $+24.99$ with two exceptions: for RSC potential ($+25.09$ in [29]) and the old MSU potential ($+25.76$, see [29] as well).

Data for T_{20} in the $C(d, p)X$ breakup from [28] are less accurate in comparison with the $p(d, p)X$ data from [27], but still can be used in order to address the question

of the T_{20} sensitivity to Coulomb effects at $k < 50 \text{ MeV}/c$ [31]. As it is shown in Fig. 6, these effects (if exist) are invisible at the present data accuracy. (In both cases we do not take into account any possible systematic uncertainties of the experiments.)

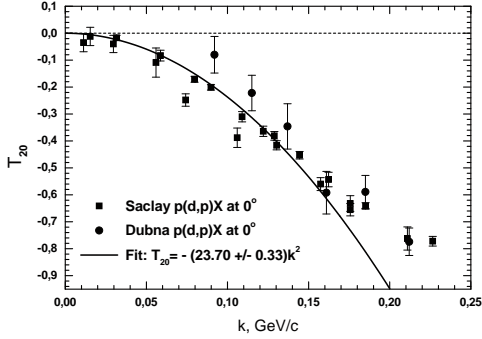


Fig. 5. Data on T_{20} from Refs. [27,28] at small k . Solid line: fit according Eq. (18) in the region of $k \leq 150 \text{ MeV}/c$.

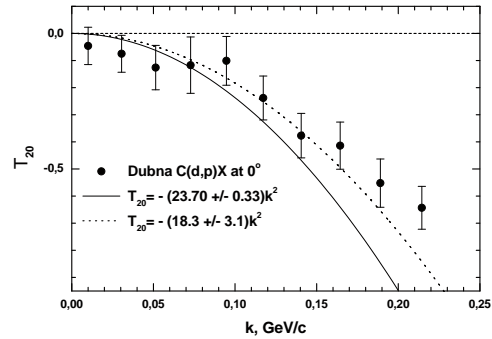


Fig. 6. Data on T_{20} from Ref. [28] at small k . The solid line is the same as in Fig. 5 (fixed D_2^d). Dotted line: similar fit to the $C(d,p)X$ data at $k \leq 150 \text{ MeV}/c$.

6 Conclusions

We have presented here an analysis of the spin-dependent observables for $(^3\text{He}, d)$, $(^3\text{He}, p)$, and (d, p) breakup reactions and obtained some rather strict relations between experimental observables at small internal momenta of fragments.

Our analysis demonstrates that the breakup reactions with the lightest nuclei at intermediate energies provide a new way for obtaining experimental data on the D_2 parameter for these nuclei, which is complementary to the usual methods, involving rearrangement reactions at low energies.

Alternatively, the (d, p) breakup reaction can be used for polarimetric purposes (for example, measurements of the deuteron beam tensor polarization) because (i) the accuracy of knowledge of the D_2^d parameter is now high enough for such purposes and (ii) the cross section of this reaction is high enough, what results in rather high “figure of merit”, almost independent upon the beam energy.

We emphasize that the different conventions regarding the angular momentum summations for the $3N$ system result in different forms for the formulae connecting spin-dependent observables with the ${}^3\text{He}$ wave function components. Of course, the final numerical results do not depend on the conventions provided that the calculations are performed systematically within one chosen scheme. However the occasional mixing of the schemes leads unavoidably to erroneous results. Therefore an explicit indication of the chosen angular momentum summation scheme is important for the applications².

Comparing the results of calculations of the deuteron and proton momentum distributions in the ${}^3\text{He}$ nucleus with existing experimental data, we conclude that the model used for the ${}^3\text{He}$ breakup reactions works reasonably well for $k \lesssim 250 \text{ MeV}/c$ but at higher momenta the data and calculations are in systematic disagreement. This disagreement, i.e., the enhancement of the experimental momentum distributions over the calculated ones above $k \approx 0.25 \text{ GeV}/c$ is very similar to the enhancement

² Perhaps the lack of such indication explains, why the sign of the D -wave, parametrized in [33] on the basis of values tabulated in [19], is opposite to that of the original tables.

of data over calculations observed for the (d, p) fragmentation [26] at small emission angles. This was interpreted for the two-nucleon system as a manifestation of the Pauli principle at the level of constituent quarks [32]. In other words, an extrapolation to this region of the wave function based on phenomenological realistic NN potentials for point-like nucleons is questionable even when relativistic effects are taken into account within the framework of light cone dynamics.

7 Acknowledgments

The authors gratefully acknowledge Yuri Uzikov and Colin Wilkin for their interest to the work and fruitful discussions on various points considered in the present paper. The work of A.P.K. was supported by the Research Programm “Research in Strong Interacting Matter and Hadron Dynamics in Relativistic Collisions of Hadrons and Nuclei” of National Academy of Sciences of Ukraine.

References

1. E. Jans et al., Phys. Rev. Lett. **49**, 974 (1982)
2. M. M. Rvachev et al., Phys. Rev. Lett. **94**, 192302 (2005).
3. C. Marchand et al., Phys. Rev. Lett. **60**, 1703 (1988)
4. R. Florizone et al., Phys. Rev. Lett. **83**, 2308 (1999)
5. V. G. Ableev et al., JETP Lett. **45**, 596 (1987) [Pis'ma v ZhETF **45**, 467 (1987)]
6. P. Kitching et al., Phys. Rev. C **6**, 769 (1972).
7. M. V. Epstein et al., Phys. Rev. C **32**, 967 (1985)
8. C. C. Kim et al., Nucl. Phys. **58**, 32 (1964); L. G. Votta et al., Phys. Rev. C **10**, 520 (1974); H. Langevin-Joliot et al., Nucl. Phys. A **158**, 309 (1970); R. Frascaria et al., Phys. Lett. B **66**, 329 (1977); P. Berthet et al., Phys. Lett. B **106**, 465 (1981)
9. Y. Shimizu et al., Phys. Rev. C **76**, 044003 (2007)
10. I. M. Sitnik et al., Phys. Rev. C **84**, 034006 (2011)
11. I. M. Sitnik et al., Nucl. Phys. A **663**, 443 (2000)
12. M. Lacombe et al., Phys. Rev. C **21**, 861 (1980)
13. R. Machleidt, Phys. Rev. C **63**, 024001 (2001)
14. V. Baru, J. Haidenbauer, C. Hanhart, and J. A. Niskanen, Eur. Phys. J. A **16**, 437 (2003)
15. A. P. Kobushkin, E. A. Strokovsky, arXiv:1204.0425 [nucl-th] (2012); to be published in Phys. Rev. C
16. W. Schadow, W. Sandhas, J. Haidenbauer, and A. Nogga, Few Body Systems **28**, 241 (2000)
17. L. D. Knutson et al., Phys. Rev. Lett. **35**, 1570 (1975)
18. J. L. Friar, B. F. Gibson, D. R. Lehman, G. L. Payne, Phys. Rev. C **25**, 1616 (1982) and references therein
19. R. Schiavilla, V. R. Pandaripande and R. B. Wiringa, Nucl. Phys. A **449**, 219 (1986)
20. A. P. Kobushkin, Deuteron-93, in *Proc. Int. Symposium “Dubna Deuteron-93”*, Dubna, Sept. 14-18, 1993, JINR, E2-94-95 (1994), p.71
21. M. E. Brandan and W. Haeberli, Nucl. Phys. A **287**, 213 (1977).
22. S. Roman et al., Nucl. Phys. A **289**, 269 (1977)
23. S. Sen and L. D. Knutson, Phys. Rev. C **26**, 257 (1982)
24. See, for example, V. G. J. Stoks et al., Phys. Rev. C **49**, 2950 (1994) and E. Epelbaum, Braz. J. Phys. **35**, 854 (2005), as well as <http://nn-online.org/>
25. I. M. Sitnik et al., JINR preprint E1-94-186 (1994); in *Proc. Int. Symposium “Dubna Deuteron-93”*, Dubna, Sept. 14-18, 1993, JINR, E2-94-95 (1994), p.282
26. V. G. Ableev et al., Nucl. Phys. A **393**, 491 (1983) and Nucl. Phys. A **411** 541 (E) (1983); V. G. Ableev et al., JINR Rapid Comm. **1[52]-92**, 10 (1992); V. G. Ableev et al., JINR Rapid Comm. **1[52]-92**, 5 (1992) and Yad. Fiz. **37**, 132 (1983) (in Russian).
27. See, for example, C. F. Perdrisat et al., Phys. Rev. Lett. **59**, 2840 (1987); V. Punjabi et al., Phys. Rev. C **39**, 608 (1989); L. S. Azhgirey et al., Phys. Lett. B **387**, 37 (1996)

28. V. G. Ableev et al., JINR Rapid Comm. **4[43]-90**, 5 (1990); first data in Pis'ma v ZhETF **47** 558 (1988); B. Kuehn et al., Phys. Lett. B **334**, 298 (1994); L. S. Azhgirey et al., JINR Rapid Comm. **3[77]-96**, 23 (1996)
29. V. M. Krasnopol'sky et al, Phys. Lett. **165B**, 7 (1985)
30. W. Grübler et al., Phys. Lett. B **92**, 279 (1980)
31. A. P. Kobushkin, Ya. D. Krivenko-Emetov, Ukr. J. Phys. **53**, 751 (2008)
32. A. P. Kobushkin, Phys. Lett. B **421**, 53 (1998); Phys. Atom. Nucl. **62**, 1140 (1999) 1140 [Yad. Fiz. **62**, 1213 (1999)]
33. J. - F. Germond and C. Wilkin, J. Phys. G: Nucl. Phys. **14**, 181 (1988).